

CathFlow: Self-Supervised Segmentation of Catheters in Interventional Ultrasound Using Optical Flow and Transformers

Alex Ranne^{1,*}, Liming Kuang^{2,*}, Yordanka Velikova^{2,*}, Nassir Navab², and Ferdinando Rodriguez y Baena¹

Abstract—In minimally invasive endovascular procedures, contrast-enhanced angiography remains the most robust imaging technique. However, it is at the expense of the patient and clinician’s health due to prolonged radiation exposure. As an alternative, interventional ultrasound has notable benefits such as being radiation-free, fast to deploy, and having a small footprint in the operating room. Yet, ultrasound is hard to interpret, and highly prone to artifacts and noise. Additionally, interventional radiologists must undergo extensive training before they become qualified to diagnose and treat patients effectively, leading to a shortage of staff, and a lack of open-source datasets. In this work, we seek to address both problems by introducing a self-supervised deep learning architecture to segment catheters in longitudinal ultrasound images, without demanding any labeled data. The network architecture builds upon AiAReSeg, a segmentation transformer built with the Attention in Attention mechanism, and is capable of learning feature changes across time and space. To facilitate training, we used synthetic ultrasound data based on physics-driven catheter insertion simulations, and translated the data into a unique CT-Ultrasound common domain, CACTUSS, to improve the segmentation performance. We generated ground truth segmentation masks by computing the optical flow between adjacent frames using FlowNet2, and performed thresholding to obtain a binary map estimate. Finally, we validated our model on a test dataset, consisting of unseen synthetic data and images collected from silicon aorta phantoms, thus demonstrating its potential for applications to clinical data in the future.

I. INTRODUCTION

Cardiovascular diseases have been a major source of concern for the WHO, claiming an estimated 17.9 million lives each year [1]. Diseases that fall into this category include vessel wall malformations, such as aneurysms and chronic occlusions, or heartbeat irregularities, just to list a few. Out of these, Abdominal Aortic Aneurysm (AAA) is especially dangerous, identified by the weakening and thinning of the abdominal aorta. In most cases, AAA is asymptomatic, but can lead to severe consequences if ruptured, resulting in a mortality rate of approximately 60% [2].

In a modern-day operating room, minimally invasive endovascular surgery (MIES) has become the norm for treating

*These authors contributed equally to this work

This work was supported by the UKRI CDT in AI for Healthcare under Grant EP/S023283/1, the ICL-TUM Joint Academy of Doctoral Studies (JADS) program, and the TUM Global Incentive Fund.

¹Alex Ranne and Ferdinando Rodriguez y Baena are with the Hamlyn Centre for Robotic Surgery, Imperial College London, SW7 2AZ, UK (e-mail: {alex.ranne17, f.rodriguez}@imperial.ac.uk) (Corresponding author: Alex Ranne)

²Liming Kuang, Yordanka Velikova, and Nassir Navab are with the Chair for Computer Aided Medical Procedures and Augmented Reality (CAMP), Technical University of Munich, 85748 Garching, Germany (e-mail: {liming.kuang, dani.velikova, nassir.navab,}@tum.de)

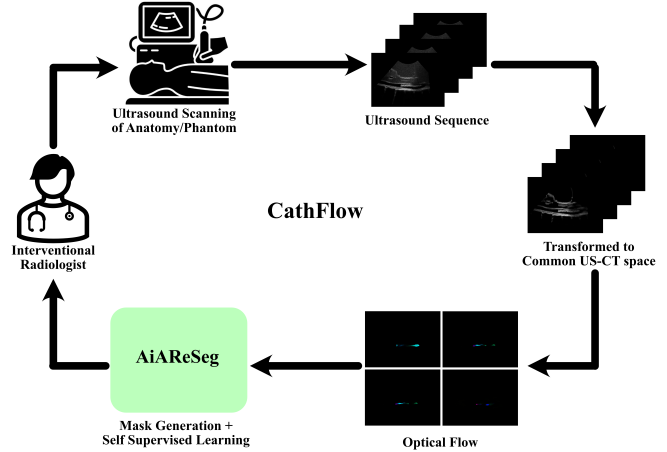


Fig. 1. Proposed Interventional Workflow when CathFlow is incorporated into the surgical workflow

such diseases. In MIES procedures, the surgeons start by making a small incision near the patient’s groin or the forearm, and a selection of dedicated instruments, such as catheters and guidewires, are manually navigated from the femoral or radial artery up to the diseased lesion under fluoroscopy. While Fluoroscopy offers the most reliable visual feedback on the position and orientation of the instruments, it emits ionising radiation, which increases the risk of cancer. Additionally, Fluoroscopy is not able to highlight soft tissues. As a result, Digital Subtractive Angiography (DSA), where radiopaque contrast agent are injected into the vasculature, is performed. The toxic nature of the contrast agent, however, constitutes a burden for the patient’s kidneys, and may lead to further complications [3].

To mitigate those risks, interventional radiologists seek alternatives, one being intraoperative Ultrasound (iUS). Traditionally, contrast-enhanced sonography has been used in endovascular aneurysm repair (EVAR) procedures to localise the landing zone for stent grafts, or for post-operative checkup, ensuring that no endoleaks, defined as blood flow into the aneurysm post stent placement, is found [4]. Similarly, a study has demonstrated the potentials of 3D US in percutaneous transluminal angioplasty (PTA), where US was able to provide sufficient anatomical information, such that it can replace Fluoroscopy in nearly all 4896 cases [5].

With that said, the main challenges of using US are also evident. Firstly, locating a catheter can be challenging, as it is a slender instrument in a large and complex anatomy. Furthermore, the quality of the image may depend on the experience of the sonographer, the depth of the scan, the

force, the orientation of the transducer to ensure good contact, and the nature of the anatomy, just to name a few [6]. In all cases, US images are prone to visual artifacts and high levels of noise, which makes them difficult to interpret.

To assist clinicians with this task, bespoke techniques have been employed to computer-assisted surgeries to extract the vasculature and the catheter. While most images are still segmented manually, deep learning-driven image segmentation has been gaining popularity over the years, as it can capture complex underlying behaviours of a scene, and have proven to be robust with different imaging settings [7], motion [8], deformation [9], and many more. With that said, acquiring a sufficiently large US dataset has proven to be difficult due to a lack of open-source datasets. Labelling such images requires expertise and is time-consuming. In addition, the difficulty in convincing clinicians and regulatory bodies to adopt iUS has also stopped many initiatives in its tracks.

In this paper, we propose a self-supervised transformer framework, trained using synthetic iUS data obtained from a CT to Ultrasound translation pipeline. We continue our exploration started from a previous work [10] and provide a solution for improving catheter segmentation in endovascular iUS images, trained from simulation and without labeling. The data is synthesised using CathSim, an open-source physics-based simulator, capable of generating mechanically realistic tissue-instrument interaction (Sect. III-A). Catheter positions during insertion are simulated, then mapped back into CT domain. Consequently, US simulations are generated from the CT labels in the domain of the Common Anatomical CT-US space (CACTUSS). Before training, motion features from adjacent frames inside of a generated US sequence are extracted using FlowNet2, then thresholded and converted to a segmentation mask (Sect. III-B). Finally, using CACTUSS images and estimated ground truth, a transformer-based segmentation network is trained (Sect. III-C), and evaluated on an unseen iUS synthetic dataset, as well as US images collected from a silicon aorta phantom (Sect. IV).

II. RELATED WORKS

A. State of the Art in Image Segmentation

1) *Deep Learning: CNN-Based Methods:* In the domain of data-driven methods, Convolutional Neural Networks (CNN) have proven to be a robust and reliable technique for automatic medical image segmentation. They demonstrate remarkable performance across different imaging modalities, such as Magnetic Resonance Imaging (MRI) [11], Fluoroscopy [12], in Computed Tomography (CT) [13], and in different clinical applications, such as segmenting vascular structures [14], [15], [16]. Out of the plethora of CNN-based architectures, U-Net [17] stands out as one of the most substantial and successful innovations in the field. It features an encoder-decoder architecture, where inside the encoder an image is progressively down-sampled using different CNN kernel sizes until a bottleneck, then upsampled in the decoder, while also combining with features of different scales extracted from the encoder. Adaptations of the U-Net, such as the nnU-Net [18], introduced an additional preprocessor

and hyper-parameter tuning framework. It allows the model to self-configure to its most appropriate settings, before it is trained and post-processed in an end-to-end fashion.

2) *Deep Learning: Transformer and Hybrid Methods:* Following the introduction of the self-attention mechanism [19], transformer architectures became pervasive across various domains in modern deep learning. Having been introduced initially by Vaswani et al. [20] in natural language processing tasks, it quickly emerged as a powerful alternative to CNNs. Following the introduction of the Vision Transformer (ViT) [21], where the authors demonstrated its ability to generalise to image patches, while retaining spatial information. Soon after, Zheng et al. proposed the Segmentation Transformer (SETR) [22], which only uses the attention mechanism together with a Sigmoid activation function to generate segmentation masks as an intermediate product of a classification task.

Upon recognising the benefits of CNN in extracting features at different scales, and the attention mechanism in finding global dependencies, a new class of transformers combining both mechanisms in a single model has emerged. The Detection Transformer (DETR) [23] used a ResNet [24] backbone and the Bipartite matching loss for detection tasks, and surpassed traditional CNN techniques such as Fast-Mask-R-CNN [25], which only relies on a region proposal network. DETR was later extended to perform panoptic segmentation with the help of an additional mask head.

B. AiAReSeg and the Attention in Attention Mechanism

An inherent characteristic of US that has currently been neglected is that it comes in the form of a sequence, where features in a past frame are propagated to the next, or different views of the same feature appear over many frames. In a clinical scenario, this may occur when the clinician is scanning along a pre-planned path or moving the probe back and forth, using information from previous frames to help locate the next ones and interpret the image.

To capture this behaviour, Ranne et al. has introduced the Attention in Attention + ResNet for Segmentation architecture (AiAReSeg) [10] which combined information from across the sequence to infer knowledge on the current frame. The architecture combines important aforementioned concepts such as feature extraction on a local scale using a CNN-based backbone, a 3-branched transformer that self-attends within the initial, intermediate, and current frame, then cross-attends between them to learn the evolution of each feature across depth or time. For mask reconstruction, features from different positions in the sequence were stacked, then performed a 3D convolution to select the features for generating the mask. Finally, the architecture relies upon the AiA module, which treats the attention map as a new feature map, then performs additional self-attention before multiplying by the value. Practically speaking, this distills distant and noisy features from the attention map.

C. Catheter Simulations and CACTUSS

As mentioned in Sect. I, obtaining accurate segmentation of US is a challenging problem, not only requiring

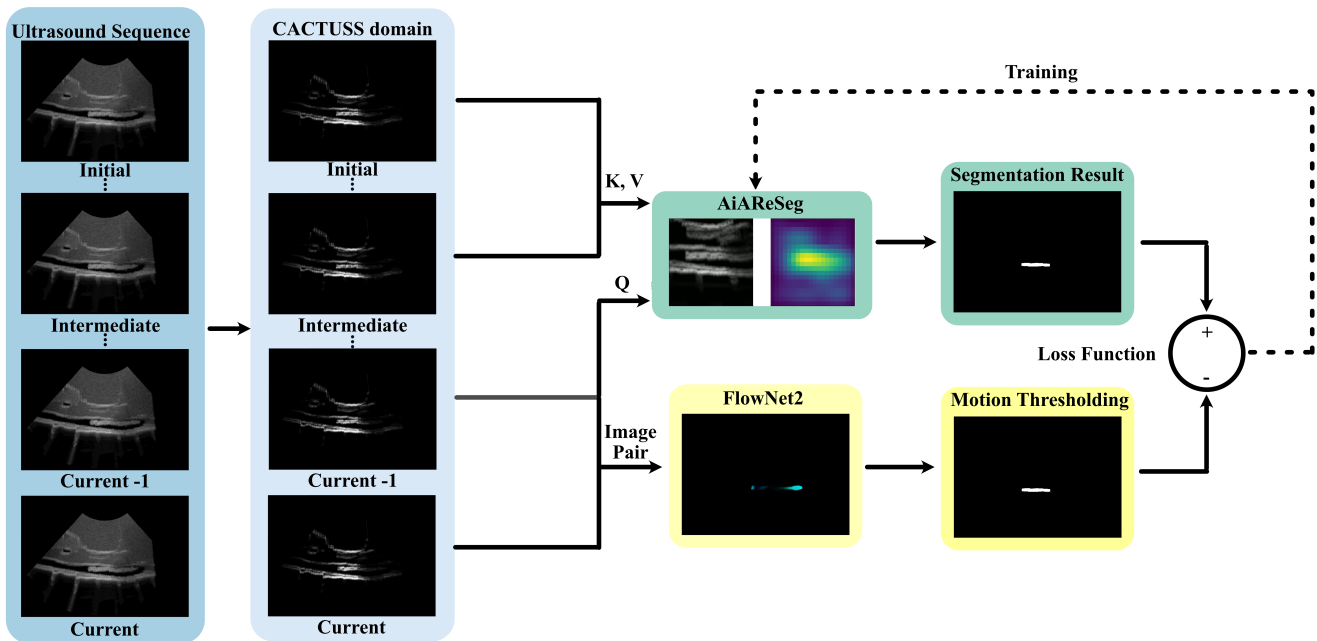


Fig. 2. Detailed pipeline of CathFlow. Representative inputs and outputs to each module is shown in the diagram.

expertise from specialists for interpretation and labelling, but also standardisation of imaging settings, operator skills, etc. Meanwhile, open-source datasets of CT images with pixel-level labels are readily available. Burger et al. developed a simulator that is capable of generating US-like images by casting rays through tissue maps, acquired from labeled CT or MRI and represent US tissue properties in every label. Ranne et al. [10] built a large dataset of axial US images from CT tissue label maps for training a catheter tracking network. In their work, an open-source catheterisation engine—CathSim [26] was used to capture the physical behaviour of catheter-tissue interaction, then the catheter positions were mapped back into CT domain, followed by the CT-US simulation.

Recently, Velikova et al. has demonstrated the use of a novel common anatomical CT-US space (CACTUSS) to improve segmentation performance [27]. They generated simulated images in a new intermediate representation, used to facilitate training. During deployment, real domain images are translated into the CACTUSS domain, where segmentation is performed. In this way, the domain gap between real and simulated images was minimised and the segmentation performance was optimised. Via visual inspection of the translation results, CACTUSS filters out unwanted domain features, such as artifacts and noise, while also standardising the image intensity distribution and texture.

D. Unsupervised motion segmentation

Catheterisation is a procedure where the MIES instruments are inserted into vasculature with guidance. Naturally, such instruments move inside of the anatomy, and their motion is captured via imaging. Capturing this motion then harnessing it for segmentation forms the core of our framework.

Inside sequences of images where the motion is consistent, optical flow can be generated, defined as the displacement of each pixel in an image relative to its adjacent image, in x and y coordinates[28]. Using this information, Meunier and Bouthemy proposed an unsupervised framework which segments key objects in a video [29]. The UNet-like network processes 3D volumes of optical flow as input and produces segmentation masks in the same form without the need for any ground truth labels. Backpropagation of the losses was performed in the optical flow space, where the final loss included a flow consistency term, and a regularisation term to ensure temporal consistency.

Another approach proposed by Choudhury et al. [30], named Guess What Moves (GWM), leverages optical flow and image features to train a per-pixel segmentation network. The architecture consists of two branches, one which predicts an initial guess of optical flow via RAFT [31], while the second is the segmentation backbone. During training, segmentation mask output proposals are provided and clustered, before being compounded into the final prediction. This prediction is used to further define the next flow estimate, producing a reconstruction flow, taking the current motion context into account for the next segmentation.

III. METHODOLOGY

A. Data Acquisition

In this work, we used two datasets. The first consists of a synthetic US dataset, simulated from CT labelmaps found in a public Synapse repository [32]. A convolutional ray-casting algorithm was used, implemented in ImFusion Suite (ImFusion GmbH, Munich, Germany). Catheterisation was simulated via an open-source simulation tool CathSim [26], where mesh models of the aorta were manually segmented

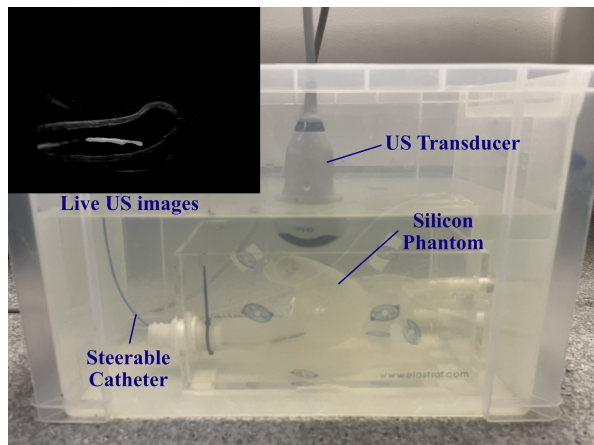


Fig. 3. Phantom setup for collecting images

and imported into CathSim to create the interactive environment. Details of the acquisition process were described in a prior work [10], with the difference of rotating the US probe angle by 90 degrees to acquire longitudinal images. Synthetic US images from 4 CT labelmaps are used for training, and 1 as a test set for evaluation. A second dataset for testing is acquired via a Zonare Z One US machine. These images are from an aorta phantom, placed in a water tank (Fig.3). Settings of the US machine were fine-tuned to minimise artifacts and noise, which resemble that of a CACTUSS domain image. Acquisition was done at a depth of 12.0cm, gain setting of G44, and frequency of 7MHz. A representative image acquired via this method is shown alongside the phantom in Fig. 3.

B. CathFlow: Self-supervised segmentation

The details of our implemented pipeline is shown in Fig. 2. CathFlow consists of 3 main components, the CACTUSS image pre-processor, the motion-to-mask ground truth estimator, and the main AiAREseg segmentation framework.

Component 1 - CACTUSS (Blue) : In this step, a ray-casting algorithm from ImFusion Suite is used to simulate US images. Input to the algorithm is a label map with 6 acoustic parameters – speed of sound c , acoustic impedance Z , attenuation coefficient α and speckle distribution parameters, which are needed to mimic the characteristics of tissues in ultrasound. With that said, simulating images with a high degree of similarity to real images does not necessarily aid segmentation performance. Hence, CACTUSS sets tissue-specific speckle parameters to zero, effectively rendering tissues black, and leaving only bright boundaries behind. When used as a pre-processing tool, CACTUSS can translate US images into an easily segmentable domain with much less noise, thereby assisting the proposed segmentation pipeline.

Component 2 - FlowNet2 and mask generation (Yellow): Since obtaining a large labelled dataset is time-consuming, we utilise motion captured with the optical flow. In this way we automatically generate labels for the images without any external input. A moving catheter inside of a stationary US image constitutes an opportunity for motion detection algorithms, such as the Farneback method [33], or networks,

such as FlowNet2 [34], RAFT [31], and PWC-Net [35] to extract optical flow from the sequence. While a detailed comparison between the aforementioned methods on our dataset can be found in Sect. IV-A, in this work we have selected FlowNet2 as the best choice due to its ability to extract large and slow-moving objects with large receptive fields, enabled by its CNN-based architecture.

The key innovation of FlowNet2 is its cascaded and deep architecture, consisting of a FlowNet-C (correlation), two FlowNet-S (simple), a FlowNet-SD (small displacement), and a Fusion block. Both FlowNet-S and FlowNet-SD consist of a standard Fully Convolutional Network (FCN) like architecture, where two adjacent frames are stacked and analysed. Here, progressively smaller kernels were used for feature extraction, and a refinement module built skip connections between the up-scaling decoder with the down-sampling encoder to supply sufficient features for flow reconstruction. On the other hand, FlowNet-C focuses on finding the correlation between two patches on the input images, defined by Eq. 1:

$$c(\mathbf{x}_1, \mathbf{x}_2) = \sum_{\mathbf{o} \in [-k, k] \times [-k, k]} \langle \mathbf{f}_1(\mathbf{x}_1 + \mathbf{o}), \mathbf{f}_2(\mathbf{x}_2 + \mathbf{o}) \rangle \quad (1)$$

Where \mathbf{f}_1 and \mathbf{f}_2 correspond to the two square image patches with center points \mathbf{x}_1 and \mathbf{x}_2 , and with the angle brackets corresponding to the convolution procedure performed in neural networks, except that the kernel is swapped for an image patch, and the patch not being trainable. The fusion block adjusts the resolution of the small displacement flow with the flow output from a cascade of FlowNet-CSS to further refine the prediction. Thereafter, a simple motion thresholding is performed to remove background noise with small motion, then the flow field is converted into a segmentation mask via a simple conditional statement, where any point in the flow field with detected motion is labelled with 1. Given an optical flow field F of size $(H, W, 2)$, where $F_{i,j} = (u_{i,j}, v_{i,j})$ represents the flow at pixel (i, j) , and a threshold value T , we define a binary segmentation mask M as follows:

$$M_{i,j} = \begin{cases} 1 & \text{if } |u_{i,j}| > T \text{ or } |v_{i,j}| > T \\ 0 & \text{otherwise} \end{cases} \quad (2)$$

Due to significant background noise, we use different thresholding values for phantom datasets compared to synthetic ones. In the following evaluation and training, if not mentioned, $T = 0.2$ for synthetic datasets and $T = 2$ for phantom datasets as default.

Component 3 - AiAREseg (Green): Given an estimation for the segmentation masks, any segmentation pipeline is theoretically applicable. However, in prior works, AiAREseg stood out as a strong contender, achieving state-of-the-art performance in axial synthetic US images. By leveraging its short-term/long-term cross-attention modules in the transformer decoder, and its 3D deconvolution in the segmentation head, we have demonstrated that the network is effective in retaining temporal or volumetric information during mask prediction, outperforming UNet and thresholding methods

that are trained on independent image-mask pairs. Thus, it was chosen to perform segmentation. Since FlowNet2 weights remain frozen, and the only element of the network that is being trained is AiARESeg, we therefore made no modification to its loss function as introduced in AiARESeg, consisting of a weighted sum of the binary cross entropy, the dice loss, and the L2 distance.

C. Data Processing

Prior to segmentation, the synthetic data is first translated to CACTUSS domain to remove intrinsic US noise, which affects the segmentation pipeline. Since the synthetic scans generate frames of moving probes with a stationary catheter, we restructure the images into folders of a moving catheter with a stationary probe to simulate catheter insertion. FlowNet2 is then deployed on the restructured dataset to generate optical flow. When there are stationary consecutive frames in a sequence, FlowNet2 will generate noisy predictions across the entire frame, while flow from frames with catheter movement would appear to be mostly clean with only significant flow signal from the catheter region. Before training, we filter out stationary frames by abusing the characteristics through thresholding. Meanwhile, we generate a bounding box for the catheter at each individual frame, in order to crop the data, such that previous predictions can help the model better divert its focus and improve the attention results. During training, data augmentations including normalization, cropping, flipping, and rotation, were introduced to boost the model’s generalisability. The same augmentation is applied to the search frame, optical flow, and reference frames.

D. Inference

Fig. 4 presents the inferencing pipeline for catheter localisation. The green section indicates the main inference loop, while the yellow section highlights how the initial frame of each inference sequence is determined. Finding the first frame containing a catheter is essential for two reasons. First, we can avoid performing inference on static frames, reducing unnecessary computations. Second, since we use the prediction from the previous frame to generate the bounding box for the current frame, it prevents the use of a wrong bounding box when a catheter appears. Bounding box quality is essential for better prediction quality, as it guides the model to focus on regions where the catheter is most likely to be.

The bounding box is generated using the same aforementioned threshold scheme (Eqn. 2), where we directly extract a bounding box for the segmented region. Since FlowNet2 is prone to produce noisy outputs for static frames, these frames can be thresholded by using $T = 0.2$ for synthetic dataset and $T = 1$ for phantom datasets. If the thresholded flow field is empty, there would be no corresponding bounding box, indicating the absence of a catheter.

Once the initial bounding box is determined, CathFlow’s inference loop is performed (blue section). The forward pass of CathFlow takes the current frame (i) and the bounding box

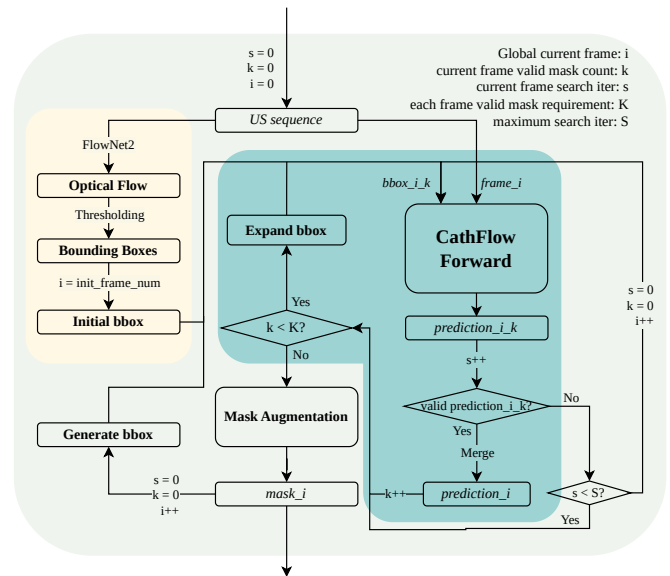


Fig. 4. The Inference Pipeline of CathFlow

of the previous segmentation as input. For each individual frame, we keep track of (s): the iteration of inference conducted, and (k): the amount of valid predictions. During inferencing, the initial bounding box is passed into CathFlow, and a prediction is obtained. If the prediction is deemed valid, we merge it to form prediction $_i$, an aggregate of valid predictions for the current frame. Else, the bounding box expands in size by a factor, which increases as s increases, and seeks to obtain a different result. This iterative process ensures that each frame’s prediction is not only built upon a foundation of reliable preceding inferences but also adheres to the set quality standards. Through the strategic expansion of the bounding box and mask augmentation, CathFlow refines its focus, thereby enhancing the localisation accuracy of the catheter in successive frames.

IV. EXPERIMENTAL EVALUATIONS

A. Optical Flow Generation

Model-based methods, including Farnebäck and deep learning-based methods including PWC-Fusion [36] (a variant of PWC-Net), RAFT, and FlowNet2 are explored for optical flow generation. All methods are evaluated on unprocessed US sequences for fairness. In Fig. 5, we demonstrate qualitative results of the performance of each method on an US sequence with a stationary probe. Farnebäck shows promise for catheter segmentation, however, the kernel size and parameters heavily impact the quality of the generated flow. Despite extensive fine-tuning, the optical flow remains to be either spotty or overly blurry. PWC-Net and PWC-Fusion are also studied, however the outputs are less than ideal. PWC-Net has a noticeably long inference time (0.75fps) compared to PWC-Fusion and less detailed outputs. PWC-Fusion is faster but it is still heavily affected by background noise, thus producing less significant flows. The most up to date optical flow prediction architecture

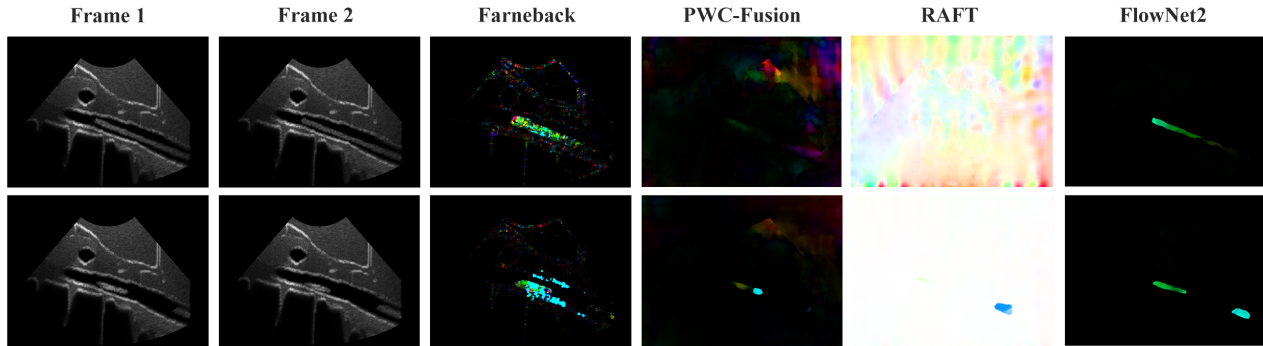


Fig. 5. Different optical flow generation methods and respective generated optical flow on ultrasound sequence.

we trialed - RAFT, has also performed poorly. Its trait of maintaining a high-resolution flow field is precisely what limits its performance. Due to the noisy nature of US, the sequence usually has large number of small displacements in the background region, leading to an unusable flow in most scenarios. In all of our tests, FlowNet2 consistently delivers the cleanest optical flow and maintains stable segmentation of the catheter. As FlowNet2 creates artificial noise in its prediction if there are no significant catheters movements in the frame, we filter small flow components out via thresholding. This feature is also utilised during inferecing to identify the initial frame where the catheter emerges.

B. Training details

Experiments were conducted on a workstation with NVIDIA GeForce RTX 4060Ti 16G, 32G RAM, and AMD Ryzen 5800X. The US simulations were generated on the ImFusion Suite, where the ray-casting algorithm was implemented. A total of 5 US scans are synthesized, each scan consists of 100 sequences, and each sequence consists of from 72 to 163 frames, sums up to a total of 66900 frames. 4 of the 5 datasets are used for training (50600 frames), and the remaining one, consisting of 16300 frames for evaluation.

C. Benchmarking details

Our model is evaluated against other similar unsupervised segmentation models including the nnU-Net [18] trained in an unsupervised fashion, and the Guess-What-Moves model [30] with MaskFormer [37] backbone. Metrics including Dice metric and mean average error (DSC) are considered.

1) *CathFlow*: Our proposed model is trained in an end-to-end fashion. Weights are initialized from a pre-trained AiArSeg model at 500 epochs. We discard the last 2 layers of the AiA transformer module and all weights in the segmentation head. CathFlow is trained for 100 epochs with a step learning rate scheduler starting at 1×10^{-3} .

2) *Guess What Moves*: We initialised the GWM model with MaskFormer as backbone with the best checkpoint provided by the author trained on DAVIS dataset. This checkpoint is further fine-tuned by the same training set used for training CathFlow for 40000 iterations with a base learning rate of 1×10^{-4} , while using an unfreeze schedule

TABLE I
EVALUATION ON SYNTHETIC DATASET

Metric	Dice Score	MAE
GWM	58.4 ± 0.213	0.1207 ± 0.1217
nnU-Net	21.6 ± 0.180	0.0056 ± 0.0009
nnU-Net*	66.7 ± 0.119	0.0032 ± 0.0014
Ours	72.8 ± 0.199	0.0022 ± 0.0020

TABLE II
EVALUATION ON PHANTOM DATASET

Metric	Dice Score	MAE
GWM	3.7 ± 0.048	0.0324 ± 0.0525
nnU-Net	3.7 ± 0.026	0.0102 ± 0.0020
nnU-Net*	2.4 ± 0.026	0.0116 ± 0.0010
Ours	41.9 ± 5.6760	0.0051 ± 0.0007

of $[(1, 10), (0, 2000), (-1, 5000)]$. Since GWM requires pairs of optical flow for training, optical flows of stride - 1 are generated using the same FlowNet2 checkpoint for all training and evaluation frames.

3) *nnU-Net*: A dynamically configured nnU-Net implemented as part of the MONAI library was used [38]. In comparison with the standard UNet, nnUNet is able to dynamically adapt its hyperparameters to best fit the task at hand. The nnUNet is trained with a learning rate of 1×10^{-5} , initialised with kernel sizes of 7, 5, 3, 3 in its encoder, with a kernel size of 2, 2, 1 in the decoder. Training was done with segmentation mask estimates generated in CathFlow.

V. RESULTS

In Tab. I and Tab. II, we present the segmentation results in the synthetic and phantom datasets, respectively. Evidently, CathFlow with its AiArSeg backbone decisively outperforms its competitors, averaging to a mean dice score of 72.8 for the synthetic case and 41.9 for the phantom case. We presented two cases of nnU-Net in this study. The first which computes the average dice metric for the complete unfiltered dataset, where US sequences may or may not contain a catheter, prompting the model to give a null prediction where there is no catheter. The second (as indicated by asterisks), is for a filtered dataset where every frame contains a catheter. As observed from Tab. I, even without significant advantages, our model still outperformed nnU-Net. Similarly, the

mean MAE across both trials also illustrated that CathFlow produces results which are geometrically closer to the ground truth in a pixel-wise manner, where CathFlow produced the lowest MAE of 0.0022 and 0.0051 in synthetic and phantom trials, respectively.

VI. DISCUSSIONS

From the results obtained in Tab. I, we have observed that CathFlow obtained the highest dice score and lowest MAE. This suggests that within the same image domain as the training set - where the images are simulated in the same manner, consisting of the same texture, and preprocessed via CACTUSS - CathFlow is able to outperform its unsupervised counterparts. Our model's main advantage lies in the AiA module design, allowing it to attend better to regions of high weights in an attention map, while ignoring noisy features that may disturb the segmentation results.

When compared with other models, it was clear that the performance improves when temporal information is utilised. First, with GWM, its approach of using a recurrent flow reconstruction as the main training signal to the segmentation network did not provide it with any advantages over our model. Thus, it can be inferred that improving the quality of the flow estimation was not able to aid the main segmentation network, and that the flows generated via FlowNet2 were sufficient to generate a single-shot estimation for our framework. Similar results were observed with the nnU-Net, with both a general unfiltered sequence and a filtered sequence with catheters in every frame. The significant drop in performance was most likely due to nnU-Net assuming that every frame contains a catheter regardless of the features presented to it, thus incorrectly assigning labels. Overall, both models in-comparison only examine features in one frame for the segmentation mask, however the temporal awareness modules in AiAReSeg, such as the LT/ST cross attention, and 3D deconvolution modules, which is able to infer the changes in the features across time, provide our model the edge. The performance of our model was limited by the splitting of mask segments created by the optical flow, which is not present in ground truth masks. Potential future works that investigate techniques to join such disjointed portions together may be explored.

Finally, an evaluation within the phantom images, has highlighted some strengths of our model, albeit also exposing several limitations. Judging by the metrics, our model still outperforms its rivals. In the case that all other models appear to not be able to segment the catheter at all, at near zero dice metrics, our model was still able to generate better results. However, a score of 41.9 indicates that the model was not able to generalise well only based on synthetic data, unlike the case of a supervised AiAReSeg model, likely due to the task of segmenting in transverse images being significantly more challenging than the axial case, and the quality of the segmentation masks obtained from optical flows. The main obstacle was that in the experiments, the catheter touches the wall, making them indistinguishable, and thus causing problems for the segmentation pipelines. In

fact, since the scanned phantom was placed in a water tank, its appearance was similar to the aesthetics of a CACTUSS image, we did not have to translate it explicitly. In the event that a full clinical dataset is obtained, we can then harness the full capability of the CACTUSS pipeline to further improve the segmentation performance, which the authors have demonstrated to successfully translate to clinical data [27].

VII. CONCLUSIONS

In this work, we present a self-supervised catheter segmentation approach in iUS-guided endovascular procedures. This framework is built upon the assumption that such image sequences consist of a stationary transducer and a moving catheter advancing through the aorta, and such motion features can be extracted as optical flows, then converted into segmentation mask estimates. We continued our previous line-of-work in synthesising catheterisation US sequences using a CT-to-US ray-casting and physics-based simulator. Then, we translated our images into the CACTUSS domain, filtering out unwanted features and easing the task. Following a qualitative comparison of the quality of the flow reconstruction, FlowNet2 was selected, as it strikes a satisfactory balance between the cleanliness of the output, and the inference speed. Using this method, we trained an improved version of AiAReSeg, and finally benchmarked its performance in both synthetic and phantom images, against state-of-the-art unsupervised frameworks, and the nnU-Net, trained in the same self-supervised manner. Our results highlighted the feasibility of the framework to translate from sim-to-real, outperforming its rivals by a substantial margin. This work presents an important milestone towards automatic labelling and segmentation in a surgical workflow, and has the potential to be integrated into MIES following fine-tuning and validation on clinical data.

REFERENCES

- [1] Joel A Kaplan. *Kaplan's cardiac anesthesia: In cardiac and noncardiac surgery*. Elsevier Health Sciences, 2016.
- [2] Brant W Ullery, Richard L Hallett, and Dominik Fleischmann. Epidemiology and contemporary management of abdominal aortic aneurysms. *Abdominal Radiology*, 43:1032–1043, 2018.
- [3] Steven D Weisbord and Paul M Palevsky. Radiocontrast-induced acute renal failure. *Journal of Intensive Care Medicine*, 20(2):63–75, 2005.
- [4] Reinhard Kopp, Werner Zürn, Rolf Weidenhagen, Georgios Meimarakis, and Dirk A Clevert. First experience using intraoperative contrast-enhanced ultrasound during endovascular aneurysm repair for infrarenal aortic aneurysms. *Journal of vascular surgery*, 51(5):1103–1110, 2010.
- [5] Masanori Wakabayashi, Sayaka Hanada, Hiroyuki Nakano, and Tsunemichi Wakabayashi. Ultrasound-guided endovascular treatment for vascular access malfunction: results in 4896 cases. *The Journal of Vascular Access*, 14(3):225–230, 2013.
- [6] Vivien Gibbs, David Cole, and Antonio Sassano. *Ultrasound physics and technology: how, why and when*. Elsevier Health Sciences, 2011.
- [7] Zhongliang Jiang, Yuan Bi, Mingchuan Zhou, Ying Hu, Michael Burke, and Nassir Navab. Intelligent robotic sonographer: Mutual information-based disentangled reward learning from few demonstrations. *The International Journal of Robotics Research*, page 02783649231223547, 2023.
- [8] Zhongliang Jiang, Hanyu Wang, Zhenyu Li, Matthias Grimm, Mingchuan Zhou, Ulrich Eck, Sandra V Brecht, Tim C Lueth, Thomas Wendler, and Nassir Navab. Motion-aware robotic 3d ultrasound. In *2021 IEEE International Conference on Robotics and Automation (ICRA)*, pages 12494–12500. IEEE, 2021.
- [9] Zhongliang Jiang, Yue Zhou, Yuan Bi, Mingchuan Zhou, Thomas Wendler, and Nassir Navab. Deformation-aware robotic 3d ultrasound. *IEEE Robotics and Automation Letters*, 6(4):7675–7682, 2021.
- [10] Alex Ranne, Yordanka Velikova, Nassir Navab, et al. Aiaresseg: Catheter detection and segmentation in interventional ultrasound using transformers. *arXiv preprint arXiv:2309.14492*, 2023.
- [11] Paolo Zaffino, Guillaume Pernelle, Andre Mastmeyer, Alireza Mehrtash, Hongtao Zhang, Ron Kikinis, Tina Kapur, and Maria Francesca Spadea. Fully automatic catheter segmentation in mri with 3d convolutional neural networks: application to mri-guided gynecologic brachytherapy. *Physics in Medicine & Biology*, 64(16):165008, 2019.
- [12] Anh Nguyen, Dennis Kundrat, Giulio Dagnino, Wenqiang Chi, Mohamed EMK Abdelaziz, Yao Guo, YingLiang Ma, Trevor MY Kwok, Celia Riga, and Guang-Zhong Yang. End-to-end real-time catheter segmentation with optical flow-guided warping during endovascular intervention. In *2020 IEEE International Conference on Robotics and Automation (ICRA)*, pages 9967–9973. IEEE, 2020.
- [13] Geert Litjens, Thijs Kooi, Babak Ehteshami Bejnordi, Arnaud Arindra Adiyoso Setio, Francesco Ciompi, Mohsen Ghafoorian, Jeroen Awm Van Der Laak, Bram Van Ginneken, and Clara I Sánchez. A survey on deep learning in medical image analysis. *Medical image analysis*, 42:60–88, 2017.
- [14] Zhongliang Jiang, Zhenyu Li, Matthias Grimm, Mingchuan Zhou, Marco Esposito, Wolfgang Wein, Walter Stechele, Thomas Wendler, and Nassir Navab. Autonomous robotic screening of tubular structures based only on real-time ultrasound imaging feedback. *IEEE Transactions on Industrial Electronics*, 69(7):7064–7075, 2021.
- [15] Deepak Mishra, Santanu Chaudhury, Mukul Sarkar, and Arvinder Singh Sooin. Ultrasound image segmentation: a deeply supervised network with attention to boundaries. *IEEE Transactions on Biomedical Engineering*, 66(6):1637–1648, 2018.
- [16] Alvin I Chen, Max L Balter, Timothy J Maguire, and Martin L Yarmush. Deep learning robotic guidance for autonomous vascular access. *Nature Machine Intelligence*, 2(2):104–115, 2020.
- [17] Olaf Ronneberger, Philipp Fischer, and Thomas Brox. U-net: Convolutional networks for biomedical image segmentation. In *Medical Image Computing and Computer-Assisted Intervention—MICCAI 2015: 18th International Conference, Munich, Germany, October 5-9, 2015, Proceedings, Part III 18*, pages 234–241. Springer, 2015.
- [18] Fabian Isensee, Paul F Jaeger, Simon AA Kohl, Jens Petersen, and Klaus H Maier-Hein. nnu-net: a self-configuring method for deep learning-based biomedical image segmentation. *Nature methods*, 18(2):203–211, 2021.
- [19] Jan K Chorowski, Dzmitry Bahdanau, Dmitriy Serdyuk, Kyunghyun Cho, and Yoshua Bengio. Attention-based models for speech recognition. *Advances in neural information processing systems*, 28, 2015.
- [20] Ashish Vaswani, Noam Shazeer, Niki Parmar, Jakob Uszkoreit, Llion Jones, Aidan N Gomez, Łukasz Kaiser, and Illia Polosukhin. Attention is all you need. *Advances in neural information processing systems*, 30, 2017.
- [21] Alexey Dosovitskiy, Lucas Beyer, Alexander Kolesnikov, Dirk Weissenborn, Xiaohua Zhai, Thomas Unterthiner, Mostafa Dehghani, Matthias Minderer, Georg Heigold, Sylvain Gelly, Jakob Uszkoreit, and Neil Houlsby. An image is worth 16x16 words: Transformers for image recognition at scale. *ICLR*, 2021.
- [22] Sixiao Zheng, Jiachen Lu, Hengshuang Zhao, Xiatian Zhu, Zekun Luo, Yabiao Wang, Yanwei Fu, Jianfeng Feng, Tao Xiang, Philip HS Torr, et al. Rethinking semantic segmentation from a sequence-to-sequence perspective with transformers. In *Proceedings of the IEEE/CVF conference on computer vision and pattern recognition*, pages 6881–6890, 2021.
- [23] Minghang Zheng, Peng Gao, Renrui Zhang, Kunchang Li, Xiaogang Wang, Hongsheng Li, and Hao Dong. End-to-end object detection with adaptive clustering transformer. *arXiv preprint arXiv:2011.09315*, 2020.
- [24] Kaiming He, Xiangyu Zhang, Shaoqing Ren, and Jian Sun. Deep residual learning for image recognition. In *Proceedings of the IEEE conference on computer vision and pattern recognition*, pages 770–778, 2016.
- [25] Ross Girshick. Fast r-cnn. In *Proceedings of the IEEE international conference on computer vision*, pages 1440–1448, 2015.
- [26] Tudor Jianu, Baoru Huang, Mohamed EMK Abdelaziz, Minh Nhat Vu, Sebastiano Fichera, Chun-Yi Lee, Pierre Berthet-Rayne, Anh Nguyen, et al. Cathsim: An open-source simulator for autonomous cannulation. *arXiv preprint arXiv:2208.01455*, 2022.
- [27] Yordanka Velikova, Walter Simson, Mohammad Farid Azampour, Philipp Paprottko, and Nassir Navab. Cactuss: Common anatomical ct-us space for us examinations. *International Journal of Computer Assisted Radiology and Surgery*, pages 1–9, 2024.
- [28] Berthold KP Horn and Brian G Schunck. Determining optical flow. *Artificial intelligence*, 17(1-3):185–203, 1981.
- [29] Etienne Meunier and Patrick Boutheymy. Unsupervised space-time network for temporally-consistent segmentation of multiple motions. In *Proceedings of the IEEE/CVF Conference on Computer Vision and Pattern Recognition*, pages 22139–22148, 2023.
- [30] Subhabrata Choudhury, Laurynas Karazija, Iro Laina, Andrea Vedaldi, and Christian Rupprecht. Guess what moves: Unsupervised video and image segmentation by anticipating motion. *arXiv preprint arXiv:2205.07844*, 2022.
- [31] Zachary Teed and Jia Deng. Raft: Recurrent all-pairs field transforms for optical flow. In *Computer Vision—ECCV 2020: 16th European Conference, Glasgow, UK, August 23–28, 2020, Proceedings, Part II 16*, pages 402–419. Springer, 2020.
- [32] Multi-atlas labeling beyond the cranial vault - workshop and challenge. <https://www.synapse.org/#!Synapse:syn3193805/wiki/89480>, 2015.
- [33] Gunnar Farneback. Two-frame motion estimation based on polynomial expansion. In *Image Analysis: 13th Scandinavian Conference, SCIA 2003 Halmstad, Sweden, June 29–July 2, 2003 Proceedings 13*, pages 363–370. Springer, 2003.
- [34] Eddy Ilg, Nikolaus Mayer, Tonmoy Saikia, Margret Keuper, Alexey Dosovitskiy, and Thomas Brox. FlowNet 2.0: Evolution of optical flow estimation with deep networks. In *Proceedings of the IEEE conference on computer vision and pattern recognition*, pages 2462–2470, 2017.
- [35] Deqing Sun, Xiaodong Yang, Ming-Yu Liu, and Jan Kautz. Pwc-net: Cnns for optical flow using pyramid, warping, and cost volume. In *Proceedings of the IEEE conference on computer vision and pattern recognition*, pages 8934–8943, 2018.
- [36] Zhile Ren, Orazio Gallo, Deqing Sun, Ming-Hsuan Yang, Erik B. Sudderth, and Jan Kautz. A fusion approach for multi-frame optical flow estimation.
- [37] Bowen Cheng, Alexander G. Schwing, and Alexander Kirillov. Pixel classification is not all you need for semantic segmentation.
- [38] M Jorge Cardoso, Wenqi Li, Richard Brown, Nic Ma, Eric Kerfoot, Yiheng Wang, Benjamin Murrey, Andriy Myronenko, Can Zhao, Dong Yang, et al. Monai: An open-source framework for deep learning in healthcare. *arXiv preprint arXiv:2211.02701*, 2022.